Carbohydrate Polymers 197 (2018) 614–622

Contents lists available at ScienceDirect

Carbohydrate Polymers

journal homepage: www.elsevier.com/locate/carbpol

Synthesis and characterization of nano fibrillated cellulose/Cu_2O films; micro and nano particle nucleation effects

Maryam Sabbaghan[a], Dimitris S. Argyropoulos[b,*]

[a] Faculty of Sciences and Institute for Advanced Technology, Shahid Rajaee Teacher Training University, PO Box 16785-163, Tehran, Iran
[b] Departments of Chemistry and Forest Biomaterials, North Carolina State University, 2820 Faucette Drive, Raleigh, 27695-8005, NC, USA

ARTICLE INFO

Keywords:
Nano-fibrillated cellulose (NFC)
Cuprous oxide
Morphology
Semiconductor
SEM
TGA
Particle nucleation mechanism

ABSTRACT

Cubic, truncated cubic and spherical nano and micro particles of Cu_2O, can be selectively deposited onto nano fibrilated cellulose gels by the modulated alkaline reduction of Cu^{2+} ions aided by the cellulose's reducing end groups. The role of the cellulose's reducing end groups and that of externally added carbohydrate reducing agents, towards inducing various Cu_2O morphologies, is discussed with respect to the detailed nucleation effects leading to micro and nano Cu_2O particle deposition on NFC. When the reducing end groups are provided only by the cellulose's chain ends, supersaturation effects seem to be affecting the Cu_2O nucleation mechanism. However, the Cu_2O nucleation considerations were altered when mobile reducing end groups were provided by adding dextrose in the system, promoting additional particle nucleation sites. Furthermore, the effort offered the possibility to quantitatively determine the number of accessible reducing end groups (-CHO) present in NFC, expressed in mmol/g. The optical properties of the created NFC/Cu_2O films were examined by UV–vis absorption measurements, revealing band gaps ranging between 2.02–2.25 eV. The accumulated understanding expands the utility window and opens new directions for the novel utilization of nano-fibrillated cellulose, and more specifically toward semiconductor applications.

1. Introduction

Our society's increased emphasis in the search for sustainable, green and eco-friendly materials has focused its efforts (amongst others) on cellulose. In this regard, nano-fibrillated cellulose (NFC) has received significant attention due to its ease of preparation, high specific surface area, high strength and stiffness, low weight and its ability to form transparent and flexible films. The structural characteristics of NFC offer nano-fibers of diameters in the range of 20–60 nm and length of several micrometers exhibiting both amorphous and crystalline domains, in a web-like structure (Abdul Khalil et al., 2014; Kalia, Boufi, Celli, & Kango, 2014; Missoum, Belgacem, & Bras, 2013).

On the other hand, metal oxides are an indispensable component of many applications (Patil et al., 2015; Park, Baker, & Somorjai, 2015; Vedrinea and Fechete, 2016;). Amongst them, abundant metal oxide particles of copper (I) (Cu_2O) offer low toxicity, high absorptivity (in the visible spectral range) with acceptable environmental characteristics. These oxides have seen applications in diverse areas, such as gas sensors (Zhang, Liu, Peng, Wang, & Li, 2006), components in magnetic storage media (Li, Gao, Murphy, & Gou, 2004), solar energy conversion devices (Hung, Tsung, Huang, & Yang, 2010), electrodes for lithium-ion batteries (Hasan, Chowdhury, & Rohan, 2010), catalysts in the conversion of CO to CO_2 (White, Yin, & Hall, 2006), the photo-decomposition of water to O_2 and H_2 (Paracchino, Laporte, Sivula, Gratzel, & Thimsen, 2011), and as facilitators in the preparation of various compounds (Kumar et al., 2016; Xu, Han, & Chi, 2010; Xu, Wang, & Zhu, 2006). Furthermore, nontoxic Cu_2O particles with no particular documented interactions with DNA, have seen significant attention as possible components in biological and medical applications (Jong and Borm, 2008).

Several methods have been developed for the preparation of cuprous oxide, including thermal, sono-chemical and chemical reduction methods as well as metal vapor synthetic approaches (Dhas and Raj, 1998; Vitulli and Bernini, 2002; Wang, Nikitin, & McComb, 2008).

Cellulose composites offer possibilities of improved optical, mechanical, thermal, electrical and biological properties (Hubbe, Rojas, Lucia, & Sain, 2008; Osong et al., 2016). When metal oxides are deposited on cellulose their tendency for self-induced aggregation can be modulated and/or prevented, allowing for the creation of specific structures of pre-determined morphologies and size (Hu, Chen, Yang, Li, & Wang, 2013).

Sedighi et al., (Sedighi, Montazer, & Samadi, 2014) have prepared

* Corresponding author.
E-mail addresses: dsargyro@ncsu.edu, dimitris.argyropoulos@ncsu.edu (D.S. Argyropoulos).

https://doi.org/10.1016/j.carbpol.2018.06.011
Received 31 March 2018; Received in revised form 13 May 2018; Accepted 2 June 2018
Available online 04 June 2018
0144-8617/

cotton/Cu_2O nano-composites by precipitating Cu_2O particles on cotton fabrics of good tensile using copper sulfate and a reducing agent (glucose) at elevated pH's. These fabrics showed considerable antibacterial behavior against *staphylococcus aureus* and *Escherichia coli* (Sedighi et al., 2014). Furthermore, the same team examined the photocatalytic activity of the cotton fabrics toward the daylight induced photo-degradation of methylene blue (Montazer, Dastjerdi, Azdaloo, & Mahmoudi Rad, 2015). Errokh et al., (Errokh et al., 2016) have investigated the controlled surface oxidation of cellulose fibers aimed to generate carboxylic acid groups on it so as to act as a binding site for the adsorption of Cu^{2+} via electrostatic coordination. Subsequently, the adsorbed Cu^{2+} ions were converted to Cu_2O by dipping the treated cotton fibers into an aqueous solution of hydrazine monohydrate or hydroxylamine (Errokh et al., 2016). In other efforts, the presence of Cu_2O nanoparticles-on functionalized cellulose-based aerogels was reported *via* the in situ deposition of Cu_2O nanoparticles (Xiuping et al., 2017). Octahedral Cu_2O nanoparticles were thus reported to be formed and anchored onto the surface and inner walls of the cellulose matrix. The cellulose-based aerogel with its 3D porous structure possessing various functional groups (e.g. $-COO^-$, $-NH_2$, $-OH$) was promoted as a micro reactor for the synthesis of octahedral Cu_2O nanoparticles (Xiuping et al., 2017).

In this effort, we examine the details of the modulated alkaline reduction of copper sulfate aimed at depositing Cu_2O onto nano-fibrillated cellulose gels. Our work is focused at revealing the role of the cellulose's reducing end groups towards inducing various Cu_2O morphologies. Finally, this is compared with the use of dextrose as an external reducing agent revealing intricate details of nucleation effects leading to micro and nano Cu_2O particle deposition on NFC.

2. Materials and methods

2.1. Materials

A sample of Nano Fibrillated Cellulose was provided by Stora Enso Corporation in the form of a gelatinous material containing approximately 5% by weight of solid polysaccharide. Dextrose, copper sulphate pentahydrate and sodium hydroxide were procured from fisher scientific. All chemicals were of the highest purity and were used thus without further purification.

2.2. Preparation of NFC/Cu_2O

Copper (II) sulfate pentahydrate was used as the copper source. Solution A containing specified concentrations of $CuSO_4{\cdot}5H_2O$ and solution B containing specified concentrations of dextrose were initially prepared (Table 1). The following solutions were used for the preparation of NFC/Cu_2O in the absence of external reducing agent (S1-7). 25 mL of copper (II) sulfate aqueous solution A (Table 1) were mixed with a suspension of 4 g of NFC (1 mmol) in 21 mL distilled water (25 mL total volume of suspension).

The following procedure was followed for the preparation of NFC/Cu_2O in the presence of external reducing agent (SD1-3). 21 mL of dextrose solution B was mixed with 4 g of NFC (1 mmol) in distilled water (25 mL total volume of suspension).

The mixture was kept under magnetic stirring so as to homogenize the suspension (30 min) and then heated to 50 °C using an oil bath. A specified amount of solid sodium hydroxide (Table 1) was added to the mixture and the suspension was heated at 80 °C for 30 min. The pH was measured at the end of the reaction (Fig. 1 in supplementary data).

The reddish suspension was then thoroughly washed to remove unreacted copper ions and base. The solid was then re-suspended (x2) in 40 mL of water each time and once in 40 mL of ethanol (96%). Finally, it was washed with 40 mL of water (x2) followed by shaking and centrifugation as specified above (Jouan centrifuge, CR 422, 3000 rpm, 5 min).

The NFC/Cu_2O composite films were prepared using a doctor blade with thickness settings of 1 mm. The resulting films were allowed to dry at room temperature. The thickness after drying was determined to be about 0.03 mm.

For the preparation of control samples S4 and SD3, 25 mL of distillated water were mixed with a suspension of 4 g of NFC (1 mmol) in 21 mL distilled water (25 mL total volume). The suspension was then heated with continuous agitation at 50 °C using an oil bath. A specified amount of solid sodium hydroxide (Table 1) was added to the mixture and the suspension and the temperature was increased to 80 °C and kept for 30 min. The product was finally washed as previously specified.

2.3. X-ray diffraction (XRD)

Wide-angle XRD patterns were collected using a Rigaku Smart Lab X-ray diffractometer using Cu target to generate the X-rays using Kα radiation (CuKα radiation, $\lambda = 0.15418$ nm) in the range of 15–65° *2θ*. The diffraction data was acquired using a step size and count time of 0.05° 2θ and 3 s/step, respectively.

2.4. Thermogravimetry (TGA)

A TA Instruments thermo-gravimetric analyzer (model Q500) was used. The temperature gradient was 10 °C/min and the flow of nitrogen was set at 50 mL/min. The weight loss (%) was determined by measuring the residual weight remaining at 600 °C.

2.5. Ion coupled plasma spectrometry (ICP)

Accurately weighed (0.3 g) film samples were dissolved using 10 mL of "Omni pure" Nitric Acid (concentrated) and heated the sample to 95 °C for approximately 30 min until the material was completely dissolved. The solution was then subjected to ICP analysis. The copper content of the solutions was determined using a Perkin-Elmer Corporation's Optima 8000 ICP Optical Emission Spectrometer.

2.6. Field-emission scanning electron microscopy (FE-SEM)

An FEI Verios 460L SEM was used to probe the microstructure of the deposited Cu_2O particles on the NFC films. The electron beam had an energy of 1 keV with a current of 50 pA and a stage bias of 500 V. The Verios allows for high resolution (0.7 nm is achievable at 1 kV) at low voltage, which allows insulating samples to be observed without the need for a conductive coating. EDS (energy dispersive X-ray spectroscopy) was also used to confirm that the visualized particles and cubes were indeed composed of Cu. As anticipated, oxygen and carbon were also detected. The size of Cu_2O particles on the SEM images were measured using image-J software.

2.7. UV–vis

Diffuse reflectance UV–vis (DR-UV–vis) spectra were acquired on a Shimadzu UV-VIS-NIR Spectrophotometer UV-3600 in the wavelength range of 300–800 nm in the solid state.

3. Results and discussion

3.1. Rational for reaction conditions and mechanism

The sought NFC/Cu_2O composite materials were synthesized by the alkaline reduction of copper sulfate using the NFC's and/or an external sugar's (dextrose) aldehyde groups as the reducing agents. The concentrations and experimental conditions specified in Table 1 describe two series of reactions labelled S (S1-7) where no external reducing agent was used, and a series SD (SD1 to SD3) where dextrose was used as the external reducing agent (Fig. 1).

Table 1
Solution concentrations, Cu^{2+}/NFC[3] ratios and other conditions used for the preparation of the various NFC/Cu_2O films. The resulting Cu loadings on the films are also shown expressed as wt%.

Sample	[$CuSO_4{\cdot}5H_2O$][a] mol/L	$CuSO_4{\cdot}5H_2O$[b] (mmol)	$CuSO_4$/NFC[c] mmol/g	[Dextrose][d] mol/L	Dextrose (mmol)	NaOH[e] (mmol)	Cu on film[f] (Weight %)	Yield[g] (%)
S1	0.58×10^{-3}	1.45×10^{-2}	0.0725	0	0	0.5	0.45	90
S2	1.16×10^{-3}	2.90×10^{-2}	0.145	0	0	1	0.76	73
S3	1.71×10^{-3}	4.30×10^{-2}	0.215	0	0	1.5	1.40	92.5
S4	5.8×10^{-3}	1.45×10^{-1}	0.725	0	0	5.7	4.22	89
S5	6.96×10^{-3}	1.74×10^{-1}	0.87	0	0	5.7	5.11	83
S6	8.70×10^{-3}	2.17×10^{-1}	1.08	0	0	5.7	6.27	86
S7	11.6×10^{-3}	2.90×10^{-1}	1.45	0	0	5.7	7.08	73
SD1	5.8×10^{-3}	1.45×10^{-1}	0.725	2.9×10^{-3}	0.06	5.7	4.76	96
SD2	11.6×10^{-3}	2.90×10^{-1}	1.45	8×10^{-3}	0.17	11	8.82	93.5
SD3	29.0×10^{-3}	7.25×10^{-1}	3.62	32×10^{-3}	0.68	27.5	20.1	97
Control S4	0	0	0	0	0	5.7	0	–
Control SD3	0	0	0	0	0	27.5	0	–

[a] Primary solution of $CuSO_4 5H_2O$ (Solution A).
[b] Amount of $CuSO_4 5H_2O$ in mixture of the reaction.
[c] 0.2 g of NFC.
[d] Primary solution of Dextrose (Solution B).
[e] Amount of NaOH in reaction mixture.
[f] Determined using ICP on the well washed solid film.
[g] Determined on the basis of $CuSO_4{\cdot}5H_2O$ used.

The homo-polysaccharide cellulose is composed of β-D-anhydro glucopyranose units (AGU) that are linked in a linear fashion by equatorial β (1 → 4) glycosidic bonds. Scheme 1 (see supplementary data file), shows the molecular structure of cellulose being composed of an abundance of primary and secondary hydroxyl groups and terminal anomeric C1 end groups that upon ring opening they offer an aldehyde (reducing end group) per cellulose chain (Wertz, Mercier, & Bedue, 2010).

It is important to also state here that the presence of a single such reducing end group per cellulose chain since the other side of each cellulose macromolecule is composed of a C4 (non-reducing end) that does not result in ring opening and the formation of an aldehyde.

The abundant hydroxyl functionalities, present on the surface of NFC, play a dual role in the reaction. Initially, it is hypothesized that these functionalities adsorb and anchor Cu^{2+} ions via electrostatic interaction and/or chelation (He, Kunitake, & Nakao, 2003; Shi et al., 2015) while they also stabilize the Cu_2O after its formation.

The reduction of Cu^{2+} ions to Cu^{+} can be depicted as follows:

$$2\ Cu^{2+} + 2\ OH^{-} + 2e^{-} \rightarrow Cu_2O + H_2O \quad \text{(i)}$$

$$RCHO + 3\ OH^{-} \rightarrow RCOO^{-} + 2H_2O + 2e^{-} \quad \text{(ii)}$$

Where RCHO: Free aldehyde of NFC cellulose chains or dextrose

The alkaline Cu^{2+} to Cu^{+} reduction occurs as per reactions (i) and (ii). The formed Cu^{+} ions combine quickly with excess OH^{-} to produce CuOH and then Cu_2O. (White et al., 2006; Paracchino et al., 2011) for these events to occur, the simultaneous dehydrogenation (ii) and oxidation of the anomeric carbon is essential, leading to the formation D-gluconate (R-COO^{-}) end groups (Scheme 1); in effect each reducing end group being stoichiometrically oxidized and consumed.

3.2. Characterization of the NFC/Cu_2O

3.2.1. X-Ray diffraction (XRD) patterns

The XRD powder pattern of a representative sample (SD3) is shown in Fig. 2. Three principal diffraction peaks are apparent at *2θ* angles between 14.5, 17.5, and 22.5 (peaks with stars in Fig. 1) reflecting the crystallographic information of 101, $10\bar{1}$ and 002 for nanocrystalline cellulose (Farahbakhsh, Shahbeigi-Roodposhti, Sadeghifar, Venditti, & Jur, 2017). The two peaks around 2θ = 14.5 and 22.5 represent the amorphous and crystalline regions of cellulose respectively (Fareezal, Izzati, Shazana, Rushdan, & Ainun, 2016). Overall the XRD pattern exhibits two main signals at 36.4 and 42.3 2θ that can be ascribed to the (111) and (200) reflections of the Cu_2O phase (Joint Committee on Powder Diffraction Standards, JCPDS05-0667) (Khan et al., 2015). No reflections due to extraneous impurities can be found in the pattern, supporting the homogeneous and pure nature of the deposited cuprous oxide. This was determined by manual peak integration of the amorphous halo under the 2θ 14.5 and the 17.5 (smoothly extended to the base line at higher angles) over the peak at 22.5.

The XRD patterns for samples S1, S2, S4 and SD2 are shown in supplementary data (Fig. 2). These patterns show that the (111) peak is the only peak that increases in relative intensity, indicating that the

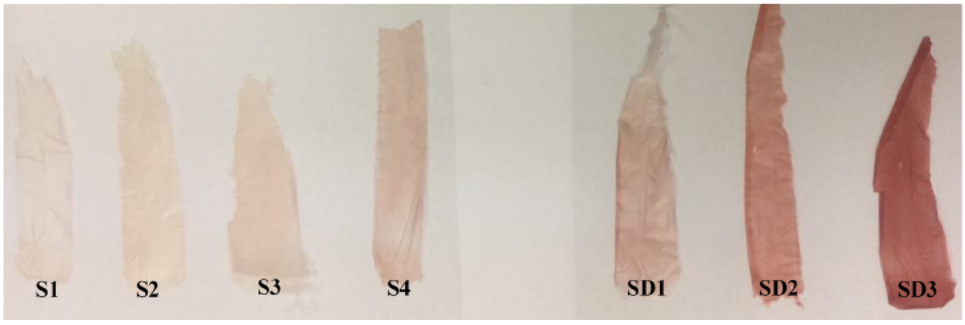

Fig. 1. The various NFC/Cu_2O films obtained during this effort. The reddish intensity is related to the amount of Cu_2O deposited.

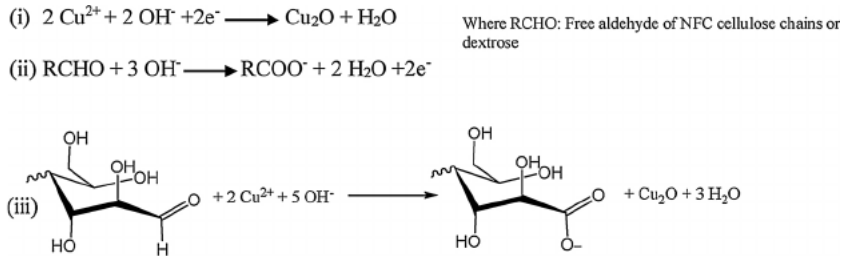

Scheme 1. Reactions operating at reducing end groups of cellulose or other carbohydrates.

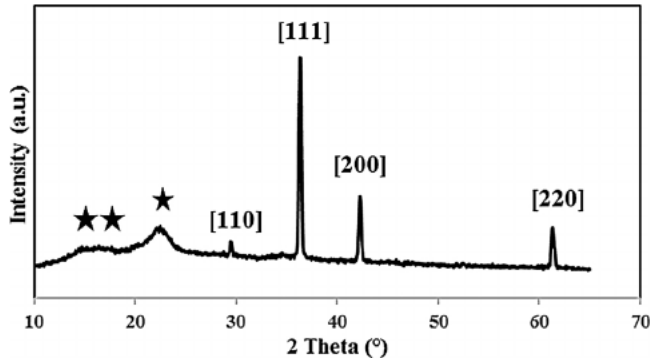

Fig. 2. XRD pattern of a representative (SD3) NFC/Cu_2O powder sample (freeze dried), the peaks with stars correspond to the NFC crystallites (see text).

crystal growth occurred along the (111) direction (Luo et al., 2005). Sample S1 showed a very weak pattern due the low concentration of Cu_2O in the sample (0.45 wt% determined by ICP).

Average crystallite sizes of products were calculated using Scherrer's formula: $D = 0.9\lambda/\beta \cos\theta$, where D is the diameter of the crystallites, λ (Cu Kα) = 1.5406 Å and β is the full-width at half-maximum of the diffraction lines (Zhou et al., 2012). The size of obtained crystallites is around 30 nm.

3.3. Thermogravimetric analyses

The thermal stability and degradation profiles of the starting NFC and NFC/Cu_2O nanocomposite films were assessed by thermal gravimetric analyses (TGA). The results of these analyses are presented in Figs. 3 and 3a-c (supplementary data). An initial small weight loss (< 5%) was detected to occur in the temperature range from 30 to 200 °C likely due to the evaporation of adsorbed water or other low molecular weight compounds from the films (Fareezal et al., 2016). The detailed major decomposition temperature regimes and the final residual mass are tabulated in Table 2. Differential thermograms (DTG) were used to evaluate peak temperatures. As such samples S1-4 and SD1-2 showed an onset decomposition temperature (T_{onset}) and a maximum degradation (T_{max}) at about 358 and 388 °C respectively, both being near the same temperature regimes for the starting NFC. However, the maximum degradation and onset temperatures were seen to be lower for the SD3 and the two control samples (Table 2). Notably the control reactions for SD3 and S4 were prepared under the same conditions of SD3 and/or S4 with the exception that cupric sulfate pentahydrate was absent (Table 1). The accumulated data implies that using high concentration of NaOH (0.55 M) used in SD3 led to a decrease in the thermal stability in the absence of Cu_2O. Sodium hydroxide was used for the reduction process (Table 2, Figure b, c supplementary data).

The decrease in the degree of crystallinity of NFC observed in the XRD patterns of the samples presented in the supplementary data supports this observation (Fig. SD3). Furthermore, Table 2 shows, the amount of the residue remaining at the end of the thermal degradation for all Cu_2O/NFC composites prepared. The most significant aspect of this data is that the residual weight of the, presumable inorganic residue, is proportional to the amount of cupric sulfate pentahydrate used and the final weight percent of copper determined on the films using ICP (Zhou et al., 2012). The largest amount of remaining residue corresponds to SD3 NFC/Cu_2O film where a large amount of dextrose and copper sulfate was used, offering a film containing about 20% by weight of copper (Table 1).

The monotonic increase of remaining residue (Table 2), that is in accord with the amount of copper sulfate and/or reducing groups used (Table 1) and the excellent qualitative correlation with the independent ICP copper measurements (Tables 1 and 2), further validate the efficiency of the washing protocol applied and many other aspects of our conclusions so far.

3.4. Determination of aldehyde end-groups present on NFC surfaces based on Cu contents

Our data, as well as the literature supports the quantitative and stoichiometric nature of the Benedict reaction (http://www.biology-discussion.com/carbohydrates/test/qualitative-and-quantitative-tests-for-carbohydrates/13042). In this respect accurate measurements of copper deposited on the cellulose films may offer a means to determine the amount of reducing (CHO =) end groups present on the cellulose we employed. To this effect we carried a series of careful experiments where the amount of copper sulphate used was systematically increased and the samples, after the Benedict reaction, were washed with extreme care so as to ensure the removal of any traces of unreacted copper. The amount of copper was then accurately determined using ICP (Table 1) and the plot of copper deposited on the cellulose as a function of copper sulphate used is shown in Fig. 4.

Apparently, the amount of copper deposited on the cellulose films is gradually increasing and then it levels off, as anticipated from the fact that the aldehyde end groups are progressively consumed. This is well demonstrated in the plot of% Cu as a function of $CuSO_4$/NFC shown in Fig. 4. By increasing the amount of $CuSO_4$ applied, per gram of NFC used, the amount of Cu deposited in the films S1 (where no external dextrose was used), the amount of the Cu_2O was progressively increasing. In an effort to determine the leveling off amount of Cu, a curve fitting function was used and the extrapolated Cu content was obtained to be 1.22 mmol/g of NFC as depicted in Fig. 4. (Note that the final data point (open circle) was obtained from the equation of the curve in Fig. 4, ($y = -1.9849 \times ^2 + 8.0338\,x - 0.2722$)).

As such, the thus determined concentration of $CuSO_4$ allowed for the accessible surface aldehyde end groups present on the NFC. More specifically, according to the mechanism presented by equation (iii) 1 mmol of aldehyde end groups requires 2 mmol of $CuSO_4$. As such it is possible to calculate the amount of aldehyde end groups present in 1 mmol of NFC.

1.22 mmol $CuSO_4$/g NFC × 1 mmol Aldehyde/2 mmol $CuSO_4$ = 0.61 mmol Aldehyde/g NFC

It is important to note here that when the experimental conditions specified for S4 in Table 1 were applied to a fully bleached softwood pulp sample no apparent reduction of Cu^{2+} to Cu^{+} occurred as

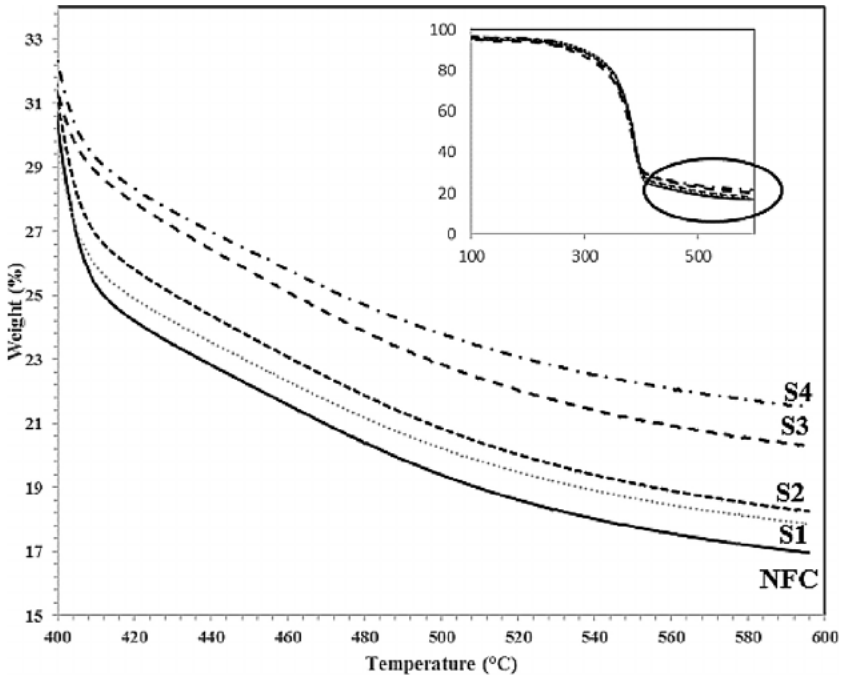

Fig. 3. Thermograms obtained for control NFC and NFC/Cu_2O composites S1-4 (see Table 1).

evidenced by the lack of Cu present on the sample and the complete lack of reddish coloration on it. This demonstrates that the amount of aldehyde end groups present on fully bleached pulp is considerably lower (since its molecular weight is apparently considerably higher) than the NFC sample used. The extensive defibration applied for the production of NFC seems to be causing significant mechanochemical degradation of the cellulose exposing a lot more reducing end groups on a per gram basis compared to a fully bleached pulp sample.

3.5. Variations on the morphology of the deposited Cu_2O; a study of micro and nano nucleation effects

The morphology of the deposited Cu_2O particles was investigated as a function of copper sulfate and dextrose concentrations using Scanning Electron Microscopy (SEM).

The SEM images of the various NFC/Cu_2O films are shown in Fig. 5 displaying the associated morphologies of the Cu_2O particles. The left column of Fig. 5 shows a series of micrographs for samples where the copper sulfate concentration varied from a low of 0.58×10^{-3} to as high as 5.8×10^{-3}mol/L (Fig. 5, S1-4 & Table 1). Not surprisingly, lower concentrations of copper cations caused the formation of Cu_2O nanoparticles of approximate size as small as 36–60 nm. These nanoparticles were likely nucleated at cellulose chain ends (Fig. 5, S1).

When the concentration of copper sulfate was increased to the point of being enough for creating the growth of larger Cu_2O crystals, a uniform cubic morphology was formed (Fig. 5, S3). More specifically, the micrographs indicate that a uniform cubic morphology for Cu_2O (Fig. 5, S3) was obtained when a 1.71×10^{-3}mol/L of copper sulfate solution was used (Table 1). SEM measurements showed that the

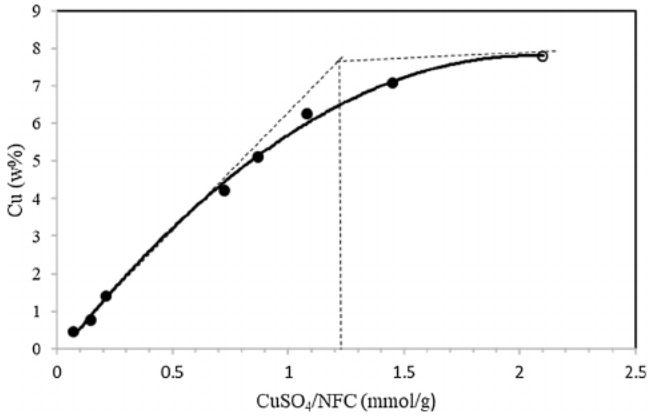

Fig. 4. The amount of Cu deposited on the various films as a function of $CuSO_4$/NFC (mmol/g). The open circled data point represents an extrapolation to determine the optimum leveling off amount of Cu. Filled circles are the experimental data while the open circle data point shown originates from the curve fit equation used (see text).

Table 2
Data extrapolated from the TGA thermograms for the synthesized NFC/Cu_2O films.

Entry	Sample	T_{onset} (°C)	T_{max} (°C)	Residue mass (%)	Wt%Cu[(1)]	Reaction pH
1	S1	359	390	17.9	0.45	11.77
2	S2	359	387	18.2	0.76	12.29
3	S3	360	387	20.3	1.40	12.72
4	S4	358	388	21.5	4.22	13.20
5	SD1	356	389	21.4	4.76	13.08
6	SD2	354	389	24.8	8.82	13.48
7	SD3	318	352	34.4	20.1	13.78
8	Starting NFC	359	389	17.0	–	–
9	Control S4	308	339	17.0	–	13.29
10	Control SD3	298	333	18.5	–	13.65

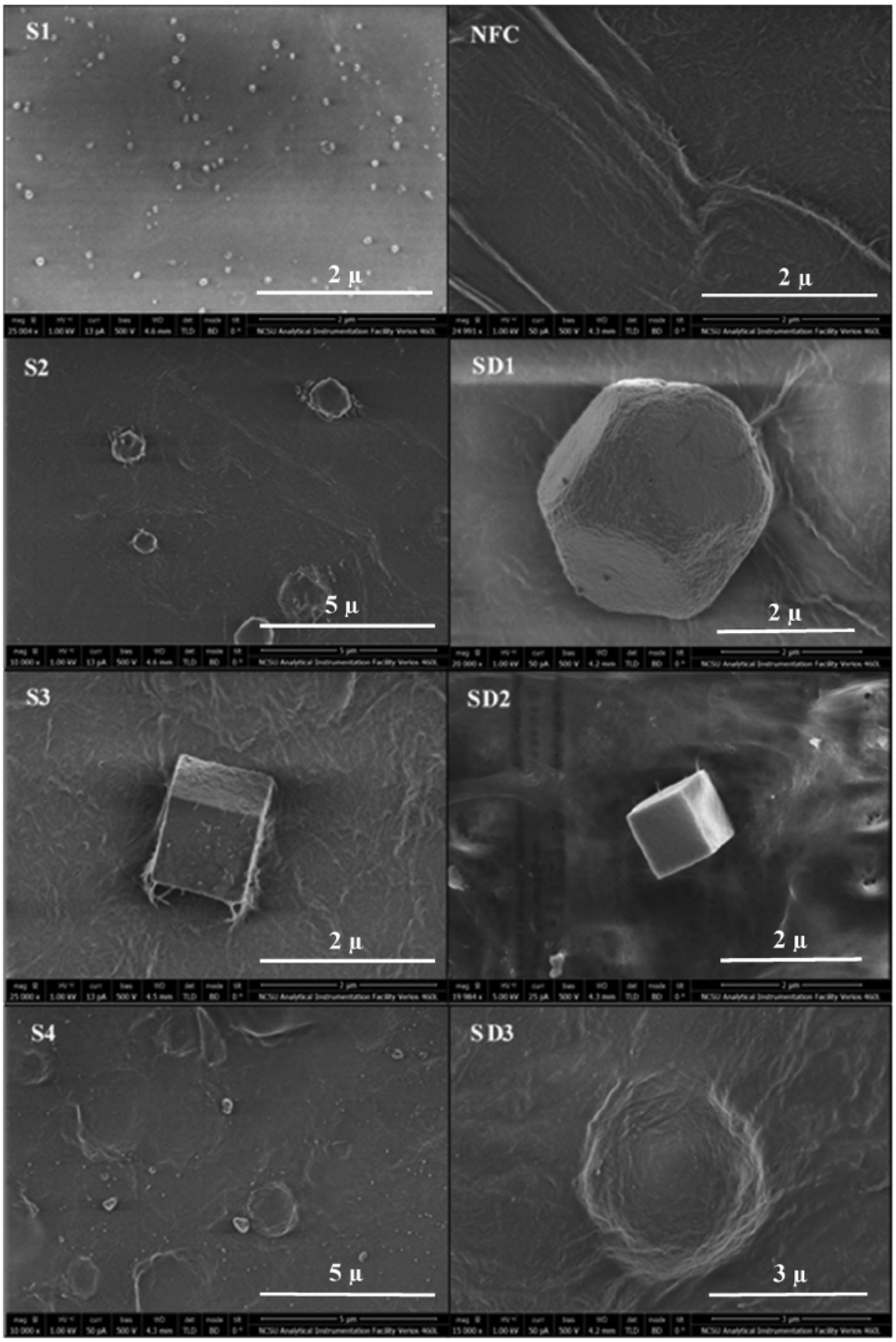

Fig. 5. FE-SEM images of the synthesized NFC/Cu_2O films in the absence of added dextrose (S series) and in its presence (SD series). As the sample number increases the amount of Cu^{2+} ions (S series) and amount of Dextrose added (SD series) are progressively increasing.

dimensions of the cube were about 1 µm.

Overall, at lower copper sulphate concentrations, non-uniform Cu_2O morphologies are apparent (sample S2 contains particles of both micro and nano dimensions).

Fig. 6 attempts to show the particle size development (bar plot) together with the associated scanning electron micrographs for samples S1-3 and SD1- SD3. Apparently for the S series of samples, obtained in the absence of added aldehyde end groups, increasing the concentration of $CuSO_4$ (see bars S1 & S2) does not alter the average Cu_2O particle size since their size remains around 1 µm. Only when the Cu ions concentration S3 is reached a uniform cube was obtained.

This observation likely sheds light on the associated mechanism of Cu_2O particle formation. At low Cu^{2+} ion concentrations the aldehyde end groups only locally create Cu_2O particles and their size remains small. Once, however, a critical concentration of Cu^{2+} ions is present (S3) the nucleated Cu_2O sites are enough to be associated together to form a uniform cubic configuration of significantly larger dimensions (about 1 µm). It is to be noted here that the aldehyde end groups in the S series is immobilized on the NFC and their amount is limited by those provided by the NFC surface.

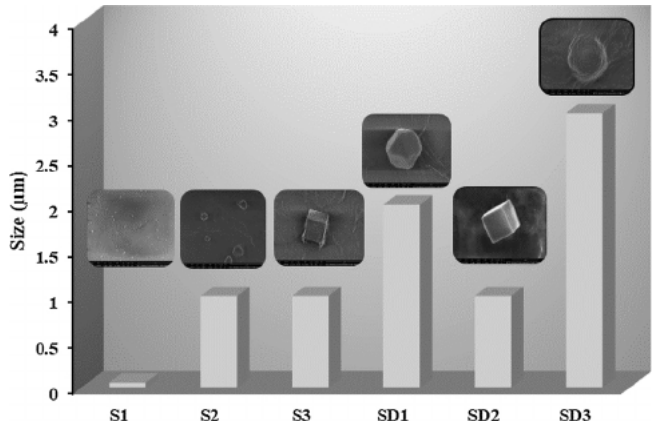

Fig. 6. Bar plots and associated scanning electron photomicrographs showing the Cu_2O particle development as a function of increasing amounts of Cu^{2+} (S1 to S3; Table 1) and as a function of increasing amounts of added aldehyde end groups in the form of added dextrose (SD1 to SD3; Table 1).

The SEM data of Fig. 5 also shows that non-uniform particles sizes (micro and nano) were obtained when concentrations of copper sulfate and sodium hydroxide higher than those used in S3 were used (S4). Literature accounts show, that the morphology and the dimensions of Cu_2O particles created by the reduction of Cu^{2+} ions is controlled by the degree of Cu^{+} supersaturation (Cao, Wang, Zhou, & Bi, 2010) in a given system. For example, Cu_2O single crystals of {111} crystallographic characteristics grow relatively fast resulting in a uniform cube. For the cube to form the crystallographic face {111} must grow via a two-dimensional growth mechanism (Cao et al., 2010). Interestingly the two-dimensional growth regime only exits for relatively narrow Cu^{+} supersaturation conditions, apparently being met under the conditions created by experiment S3 in the present effort. The higher Cu^{2+} concentration used in S4 (approximately 3.3 times greater than that used in of S3) and the ensuing higher Cu^{+} supersaturation, caused the formation of spherical and not cubic Cu_2O particles of variable sizes as likely dictated by localized association growth modes. Overall, under high supersaturation conditions, Cu_2O nucleation is an extraordinarily non-linear and fast process (Cao et al., 2010). Under such conditions, effective collisions among single-nuclei likely form molecular clusters that are the cause of primary particle aggregation, effectively leading to the growth of spherical particles (Cao et al., 2010).

To further comprehend the Cu_2O deposition process we also examined the modulated reduction of Cu^{2+} to Cu^{+} by the addition of mobile aldehyde reducing groups in the form of dextrose, creating the SD series of NFC/Cu_2O films (Table 1 and Figs. 5 and 6). By offering additional reducing end groups for the reduction of Cu^{2+} to Cu^{+} the concentration and immobilization limitations, imposed by the NFC surface were thus eliminated. The ensuing morphologies of the SD1-3 series when examined by SEM, offered the possibility of formation of larger and more uniform particles than in the S series (Figs. 5 and 6). For verification purposes, electron diffraction X ray analyses conducted on the image of sample SD3, confirmed that the composition of the deposited particles were mainly copper and oxygen. Some carbon was also present since these particles were anchored onto the cellulose backbone. (Additional SEM images of samples are included as supplementary data together with associated EDAX spectra, (Supplementary Figs. 4, 5)). These images are aimed to demonstrate the representative and holistic nature of our conclusions.

For the SD series, it seems that the presence of additional mobile reducing end groups, provided by dextrose, likely promotes additional particle nucleation sites. Furthermore, the supersaturation limitations enumerated and discussed for the S series also seem to be overcome.

Literature accounts offer information on shape direction agents (known as capping agents) that help guide the formation of certain crystal shapes (Qi, Balankura, Zhou, & Fichthorn, 2015). Surfactant molecules such as CTAB (cetyl trimethyl ammonium bromide) or p-octyl polyethylene glycol phenyl ether have been used in the preparation of different Cu_2O morphologies (Dong, Li, Wang, Cui, & Deng, 2001). Furthermore, organic or inorganic additives have been invoked to preferentially adsorb more strongly onto certain crystallographic planes effectively promoting uniform particle shape growth rates via a specific crystallographic plane, and by suppressing other growth modes (Sui et al., 2010).

Of particular interest to our work, is the effort of Sabbaghan et al., where the morphologies of Cu_2O particles (produced by the reduction of Cu^{2+}) were examined in the presence of different carbohydrates (Sabbaghan, Beheshtian, & Niazmand Liarjdame, 2015). Their account concludes that at specific aqueous concentrations various carbohydrate molecules do not only function as reducing agents but also act as shape directing agents offering Cu_2O particles of different morphologies. The accumulated data provided herein by the SD series of experiments further supports the conclusions of Sabbaghan et al. since the addition of mobile dextrose reducing end groups offered different particle shapes. For example, cubic Cu_2O particles were obtained under the conditions of SD2 while uniform spherical morphologies (of approximate diameter 3 µm) were apparent under the conditions of SD3 (Table 1, Figs. 5 and 6). Interestingly, the SD1 experimental conditions used for the Cu_2O particle deposition were identical to those of S4. However, significant differences in particle morphologies were apparent. More specifically, for S4, produced in the absence of externally added mobile reducing agent, the Cu_2O particles were non-uniform and small while in the presence of added dextrose (SD1 conditions) uniform particles of a truncated cube morphology were obtained. Apparently, variations in the amount of mobile dextrose available promote Cu_2O crystal growth containing different ratios of {111}/{100} crystallographic planes. Zhang et al. have attributed this to possible selective surface stabilization effects of the polymer they examined (Zhang et al., 2009). Dextrose can be selectively adsorbed on the {100} plane facilitating the growth on the {111} plane. Variations in the dextrose concentration offered variations in particle morphologies, namely, cubic for SD2 and spherical for SD3. The spherical particles were seen to be generated when the dextrose concentration was rather high (Table 1). This is likely due to the high and uniform availability of reducing end groups on all crystallographic planes of the growing Cu_2O crystals thus promoting uniform two dimensional crystal growth as opposed to growth based on aggregation considerations (Farahbakhsh et al., 2017). In other words dextrose plays two roles in this reaction; as a reducing agent and as “a template agent” promoting the different morphologies observed.

3.6. Band gap determinations for the prepared NFC/Cu_2O films

The energy gap between valence and conduction bands is of fundamental importance in determining optical and electrical properties of a solid such as intrinsic conductivity, optical or electronic transitions. Alterations in the band gap may significantly alter the material physically and chemically. The band gap energies can be determined from the corresponding absorption edges according to the equation (Sedighi et al., 2014)

$$Eg = 1240\ \lambda^{-1}$$

Where Eg is the band-gap energy (eV) and λ is the wavelength (nm). Cuprous oxide is a p-type semiconducting material having direct band gap of nearly 2.17 eV.

In our efforts to determine the band gap of the synthesized Cu_2O films we used solid state UV–vis spectroscopy (see Experimental & Fig. 6 in supplementary data).

Overall, the Cu_2O/NFC films containing lower amounts of Cu_2O (S1-

Table 3
Absorption edge and band gap energies obtained for the various NFC/Cu_2O films samples using diffuse reflectance Uv/Vis spectroscopy data samples.

Entry	Sample 1	Wt%Cu (1)	Absorption edge (nm)	Band gap energy (eV)
1	S1	0.45	–	–
2	S2	0.76	550	2.25
3	S3	1.40	575	2.16
4	S4	4.22	604	2.05
5	SD1	4.76	609	2.03
6	SD2	8.82	610	2.03
7	SD3	20.1	615	2.02
10	Control SD3	–	–	–

4) displayed lower UV–vis absorption at a given wavelength than the SD series of films. The absorption edge for S4 appeared at 604 nm while the band edge for samples S1 to S3 shifted to shorter wavelengths like 575 and 550 nm (Fig. 6a in supplementary data, Table 3). The higher the amount of deposited copper present in the films resulted in somewhat higher absorption edges and lower associated band gap energies (Table 3).

The solid state diffuse reflectance UV–vis spectra of NFC/Cu_2O films prepared in the presence of added dextrose (SD1-3) are also shown in (Fig. 6b in supplementary data) The absorption edge for film SD1 appeared at 609 nm while the band edge for all samples SD2 and SD3 shifted to somewhat longer wavelengths (Table 3). These values are consistent with those reported elsewhere (Sui et al., 2010; Kuo, Chen, & Huang, 2007). In a manner similar to the S series the higher the amount of deposited copper present in the films resulted in somewhat higher absorption edges and marginally lower associated band gap energies (Table 3).

Overall, a progressive decrease in the band gap (Eg value) is seen for all NFC/Cu_2O that effectively extends the absorption edge into the IR region as anticipated by the morphology and size of Cu_2O (Sabbaghan et al., 2015; Ravichandran, Dhanabalan, Vasuhi, Chandramohan, & Mantha, 2015). Different size and morphology of the samples that effect on the band gap was shown in Fig. 6. These result shows that these films have appropriate properties in solar cell application (Kimura, Moniz, Tang, & Parkin, 2015).

4. Conclusions

Cubic, truncated cubic and spherical particles of Cu_2O, ranging from micro to nano dimensions can be deposited onto nanofibrilated cellulose gels by the modulated alkaline reduction of Cu^{2+} ions aided by the cellulose's reducing end groups. When the reducing end groups are provided solely by the cellulose's chain ends, supersaturation effects seem to be affecting the Cu_2O nucleation. At low Cu^{2+} ion concentrations, the aldehyde end groups immobilized on the NFC surface, only locally create Cu_2O particles and their size remains small. Once, however, a critical concentration of Cu^{2+} ions is present the nucleated Cu_2O sites are enough to be associated together to form a uniform cubic configuration of significantly larger dimensions.

The Cu_2O nucleation considerations were altered when externally mobile reducing end groups were provided by adding dextrose in the system, likely promoting additional particle nucleation sites. Apparently, variations in the amount of mobile dextrose available promotes Cu_2O crystal growth containing different ratios of {111}/{100} crystallographic planes. It is likely that dextrose can be selectively adsorbed on the {100} plane facilitating the growth on the {111} plane. Spherical particles were generated when the dextrose concentration was rather high likely due to the high and uniform availability of reducing end groups on all crystallographic planes of the growing Cu_2O crystals, promoting uniform two dimensional crystal growth as opposed to growth based on aggregation considerations.

Author contributions

The manuscript was written through contributions of all authors. All authors have given approval to the final version of the manuscript.

Acknowledgments

The authors gratefully acknowledge Stora Enso corporation for kindly providing a sample of Nano fibrillated cellulose used in this work. MS wish to thank the Shahid Rajaee Teacher Training University, for providing the essential financial support for their visit to the laboratories of professor Argyropoulos at NCSU under contract number 14053.

Appendix A. Supplementary data

Supplementary data associated with this article can be found, in the online version, at https://doi.org/10.1016/j.carbpol.2018.06.011.

References

http://www.biologydiscussion.com/carbohydrates/test/qualitative-and-quantitative-tests-for-carbohydrates/13042.
Abdul Khalil, H. P. S., Davoudpour, Y., Nazrul Islama, M., Mustapha, A., Sudeshd, K., Dungania, R., et al. (2014). Production and modification of nanofibrillated cellulose using various mechanical processes: A review. *Carbohydrate Polymers, 99*, 649–665.
Cao, Y., Wang, Y.-, Zhou, K.-, & Bi, Z. (2010). Morphology control of ultrafine cuprous oxide powder and its growth mechanism. *Transactions of Nonferrous Metals Society of China, 20*, 216–220.
Dhas, N. A., & Raj, C. P. (1998). Synthesis, characterization, and properties of metallic copper nanoparticles. *Chemistry of Materials, 10*, 1446–1452.
Dong, Y., Li, Y., Wang, C., Cui, A., & Deng, Z. (2001). Preparation of cuprous oxide particles of different crystallinity. *Journal of Colloid and Interface Science, 243*, 85–89.
Errokh, A., Ferraria, A. M., Conceic¸ D. S., Vieira Ferreira, L. F., Botelho do Re, A. M., Rei Vilar, M., et al. (2016). Controlled growth of Cu_2O nanoparticles bound to cotton fibres. *Carbohydrate Polymers, 141*, 229–237.
Farahbakhsh, N., Shahbeigi-Roodposhti, P., Sadeghifar, H., Venditti, R. A., & Jur, J. S. (2017). Effect of isolation method on reinforcing capability of recycled cotton nanomaterials in thermoplastic polymers. *Journal of Materials Science, 52*, 4997–5013.
Fareezal, A. W., Izzati, M. A., Shazana, M. Z., Rushdan, I., Rosazley, & Ainun, Z. M. (2016). Ainun characterization of nanofibrillated cellulose produced from oil palm empty fruit bunch fibers (OPEFB) using ultrasound. *Journal of Contemporary Issues and Thought, 6*, 30–37.
Hasan, M., Chowdhury, T., & Rohan, J. F. (2010). Nanotubes of core/shell Cu/Cu_2O as anode materials for Li-ion rechargeable batteries. *Journal of the Electrochemical Society, 157*, A682–A688.
He, J. H., Kunitake, T., & Nakao, A. (2003). Facile in situ synthesis of noble metal nanoparticles in porous cellulose fibers. *Chemistry of Materials, 15*, 4401–4406.
Hu, W., Chen, S., Yang, J., Li, Z., & Wang, H. (2013). Functionalized bacterial cellulose derivatives and nanocomposites. *Carbohydrate Polymers, 101*, 1043–1060.
Hubbe, M. A., Rojas, O. J., Lucia, L. A., & Sain, M. (2008). Cellulosic nanocomposites: A review. *BioResources, 3*, 929–980.
Hung, L. I., Tsung, C. K., Huang, W. Y., & Yang, P. D. (2010). Room-temperature formation of hollow Cu_2O nanoparticles. *Advanced Materials, 22*, 1910–1914.
Jong, W. H. D., & Borm, P. J. (2008). Drug delivery and nanoparticles: Applications and hazards. *International Journal of Nanomedicine, 3*, 133–149.
Kalia, S., Boufi, S., Celli, A., & Kango, S. (2014). Nanofibrillated cellulose: Surface modification and potential applications. *Colloid and Polymer Science, 292*, 5–31.
Khan, M. A., Ullah, M., Iqbal, T., Mahmood, H., Khan, A. A., Shafique, M., et al. (2015). Surfactant assisted synthesis of cuprous oxide (Cu_2O) nanoparticles via solvothermal process. *Nanoscience and Nanotechnology Research, 3*, 16–22.
Kimura, S. M. H., Moniz, S. J. A., Tang, J., & Parkin, I. P. (2015). A method for synthesis of renewable Cu_2O junction composite electrodes and their photoelectrochemical properties. *ACS Sustainable Chemistry & Engineering, 3*, 710–717.
Kumar, S., Parlett, C. M. A., Isaacs, M. A., Jowett, D. V., Douthwaite, R. E., Cockett, M. C. R., et al. (2016). Facile synthesis of hierarchical Cu_2O nanocubes as visible light photocatalysts. *Applied Catalysis B, 189*, 226–232.
Kuo, C. H., Chen, C. H., & Huang, M. H. (2007). Seed-mediated synthesis of monodispersed Cu_2O nano cubes with five different size ranges from 40 to 420 nm. *Advanced Functional Materials, 17*, 3773–3780.
Li, X. D., Gao, H. S., Murphy, C. J., & Gou, L. F. (2004). Nanoindentation of Cu_2O nanocubes. *Nano Letters, 4*, 1903–1907.
Luo, F., Wu, D., Gao, L., Lian, S., Wang, E., Kang, Z., et al. (2005). Shape-controlled synthesis of CuO nanocrystals assisted by Triton X-100. *Journal of Crystal Growth, 285*, 534–540.
Missoum, K., Belgacem, M. N., & Bras, J. (2013). Nanofibrillated cellulose surface modification: A review. *Materials, 6*, 1745–1766.
Montazer, M., Dastjerdi, M., Azdaloo, M., & Mahmoudi Rad, M. (2015). Simultaneous synthesis and fabrication of nano Cu_2O on cellulosic fabric using copper sulfate and

glucose in alkali media producing safe bio- and photoactive textiles without color change. *Cellulose, 22*, 4049–4064.
Osong, S. H., Dahlstrom, C., Forsberg, S., Andres, B., Engstrand, P., Norgren, S., et al. (2016). Nanofibrillated cellulose/nanographite composite films. *Cellulose, 23*, 2487–2500.
Paracchino, A., Laporte, V., Sivula, K., Gratzel, M., & Thimsen, E. (2011). Highly active oxide photocathode for photoelectrochemical water reduction. *Nature Materials, 10*, 456–461.
Park, J. Y., Baker, L. R., & Somorjai, G. A. (2015). Role of hot electrons and metal-oxide interfaces in surface chemistry and catalytic reactions. *Chemical Reviews, 115*, 2781–2817.
Patil, S. J., Patil, A. V., Dighavkar, C. G., Thakare, K. S., Borase, R. Y., Nandre, S. J., et al. (2015). Semiconductor metal oxide compounds based gas sensors: A literature review. *Frontiers of Materials Science, 9*, 14–37.
Qi, X., Balankura, T., Zhou, Y., & Fichthorn, K. A. (2015). How structure-directing agents control nanocrystal shape: Polyvinylpyrrolidone-mediated growth of Ag nanocubes. *Nano Letters, 15*, 7711–7717.
Ravichandran, A. T., Dhanabalan, K., Vasuhi, A., Chandramohan, R., & Mantha, S. (2015). Morphology, bandgap, and grain size tailoring in Cu_2O thin film by SILAR method. *IEEE Transactions on Nanotechnology, 14*, 108–112.
Sabbaghan, M., Beheshtian, J., & Niazmand Liarjdame, R. (2015). Preparation of Cu_2O nanostructures by changing reducing agent and their optical properties. *Materials Letters, 153*, 1–4.
Sedighi, A., Montazer, M., & Samadi, N. (2014). Synthesis of nano Cu_2O on cotton: Morphological, physical, biological and optical sensing characterizations. *Carbohydrate Polymers, 110*, 489–498.
Shi, Z., Tang, J., Chen, L., Yan, C., Tanvir, S., Anderson, W. A., et al. (2015). Enhanced colloidal stability and antibacterial performance of silver nanoparticles/cellulose nanocrystal hybrids. *Journal of Materials Chemistry B, 3*, 603–611.
Sui, Y., Fu, W., Yang, H., Zeng, Y., Zhang, Y., Zhao, Q., et al. (2010). Low temperature synthesis of Cu_2O crystals: Shape evolution and growth mechanism. *Crystal Growth & Design, 10*, 99–108.
Vedrinea, J. C., & Fechete, I. (2016). Heterogeneous partial oxidation catalysis on metal oxides. *Comptes Rendus Chimie, 19*, 1203–1225.
Vitulli, G., & Bernini, M. (2002). Nanoscale copper particles derived from solvated Cu atoms in the activation of molecular oxygen. *Chemistry of Materials, 14*, 1183–1186.
Wang, Y. Q., Nikitin, K., & McComb, D. W. (2008). Fabrication of Au-Cu_2O core-shell nanocube heterostructures. *Chemical Physics Letters, 456*, 202–205.
Wertz, J. L., Mercier, J. P., & Bedue, O. (2010). *Cellulose science and technology*. Lausanne: EFPL Press.
White, B., Yin, M., & Hall, A. (2006). Complete CO oxidation over Cu_2O nanoparticles supported on silica gel. *Nano Letters, 6*, 2095–2098.
Xiuping, S., Qian, L., Lin, L., Ranju, M., Zhouqi, Q., Huiying, G., et al. (2017). Cu_2O nanoparticle-functionalized cellulose-based aerogel as high-performance visible-light photocatalyst. *Cellulose, 24*, 1017–1029.
Xu, H. L., Wang, W. Z., & Zhu, W. (2006). Shape evolution and size-controllable synthesis of Cu_2O octahedra and their morphology-dependent photocatalytic properties. *Journal of Physical Chemistry B, 110*, 13829–13834.
Xu, C. H., Han, Y., & Chi, M. Y. (2010). Cu_2O-based photocatalysis. *Progress in Chemistry, 22*, 2290–2297.
Zhang, J. T., Liu, J. F., Peng, Q., Wang, X., & Li, Y. D. (2006). Nearly monodisperse Cu_2O and CuO nanospheres: Preparation and applications for sensitive gas sensors. *Chemistry of Materials, 18*, 867–871.
Zhang, D. F., Zhang, H., Guo, L., Zheng, K., Han, X.-D., & Zhang, Z. (2009). Delicate control of crystallographic facet-oriented Cu_2O nanocrystals and the correlated adsorption ability. *Journal of Materials Chemistry, 19*, 5220–5225.
Zhou, P., Wang, H., Yang, J., Tang, J., Sun, D., & Tang, W. (2012). Bacteria cellulose nanofibers supported palladium (0) nanocomposite and its catalysis evaluation in heck reaction. *Industrial & Engineering Chemistry Research, 51*, 5743–5748.